CHEMICAL ENGINEERING TRANSACTIONS
VOL. 67, 2018
A publication of AIDIC
The Italian Association of Chemical Engineering
Online at www.aidic.it/cet
Guest Editors: Valerio Cozzani, Bruno Fabiano, Davide Manca

ISBN 978-88-95608-64-8; **ISSN** 2283-9216

Visualization of Aluminum Dust Flame Propagation in a Square-Section Tube

Clement Chanut*, Frederic Heymes, Pierre Lauret, Pierre Slangen

LGEI, IMT Mines Ales, Univ Montpellier, Ales, France
clement.chanut@mines-ales.fr

Metallic dust explosion is a challenging research topic. One key point of investigation is the flame propagation velocity, which can be determined experimentally by direct visualization of the explosions. This paper presents the results of flame propagation during an aluminum dust explosion inside a vertical prototype of 700 mm height and 150x150 mm square cross section, with glass walls. The study considers direct visualization: the light emitted by the aluminum flame is recorded with a fast camera. Aluminum flames look white and highly luminous. A special attention is therefore requested to collect images without saturation. Indeed, aluminum flame images from literature are mostly saturated; therefore comparison of images obtained with and without saturation is of high interest. The flame propagation velocity, which corresponds to the flame speed in the laboratory referential, is determined from saturated and non-saturated images. The burning velocity, i.e. the consumption rate of the reactants by the flame front, is then presented. With saturated images, the flame surface area is under-estimated, around 10-20 %, yielding to over-estimated burning velocity.

1. Introduction

Dust explosion is of major concern in industries dealing with powders and dusts, as all combustible dusts can cause an explosion. A large variety of dusts are combustible. These can be divided in three main categories: natural organic (corn, carbon, sugar…), synthetic organic (plastics, pigments…) and metals (aluminum, magnesium…). So, many different kind of industries has to deal with this hazard, and consequently to model the consequences of such explosions (thermal effects, overpressure and missile effects). Conversely to gas explosions, dust explosions mechanisms are not yet well understood because of an intrinsic difficulty to experimentally study these explosions: dust has to be dispersed before the ignition of the cloud to cause an explosion. For organic dust, models based on gas explosion exist to predict the consequences of such an explosion. However, they seem not accurate for metal dust explosions (Khalili, 2012). For such explosions, experimental studies are required to understand the phenomenon of flame propagation inside the dust cloud.
Several previous studies aimed to characterize the sensitivity and severity parameters, using standardized setups like the Hartmann Tube or the 20 L-sphere (Dufaud et al., 2012). These parameters are useful for risk analysis in the industry but they are not sufficient to accurately model this phenomenon through numerical simulation. Other studies, including the present paper, focus on the flame propagation, investigating the visualization of the flame profile and its evolution versus time (Di Benedetto et al., 2011; Gao et al., 2014; Proust and Veyssiere, 1988; Torrado et al., 2017). However, because metallic dust explosions are very luminous phenomenon, some images from the literature are saturated, as shown in Figure 1 (Ding et al., 2010). This can cause misinterpretation of the images, and therefore difficulties for the comprehension of the flame propagation mechanism.
In this study, saturated and non-saturated images of aluminum dust flame propagation are compared. First, the flame propagation velocity, which corresponds to the flame speed in the laboratory referential, is determined with both images (saturated and non-saturated). This velocity is dependent on the geometry of the apparatus used for his determination. For this reason another parameter has been determined: the burning velocity, which corresponds to the consumption rate of the reactants by the flame front. The determination of this velocity also requires among other the determination of the propagation velocity and the flame surface to be calculated.

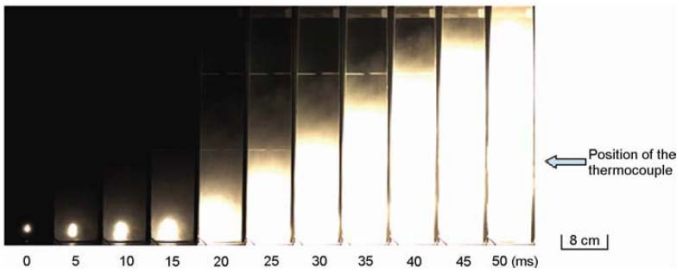

Figure 1: Saturated images of Zirconium dust flame propagation obtained by Ding et al. (2010)

2. Materials and Methods

For this study a dedicated prototype has been especially designed and manufactured. The observation chamber of the prototype is a vertical tube of 700 mm height and 150x150 mm square cross section. Walls are made of clear glass (thickness: 10 mm) to allow the visualization of the flame propagation. The dust is spread out by the discharge of two 1-liter compressed air vessels inside four vertical dust injection tubes, located in the corners of the tube (Figure 2). The dispersion tubes have an internal diameter of 7 mm and have a row of holes of 1.5 mm, along their heights. Two of these tubes disperse the dust in the bottom part of the tube; whereas the others disperse it only in the upper part (because they have no holes in the bottom part). These tubes allow a good homogeneity in terms of concentration along prototype height: the homogeneity has been estimated by Mie scattering technique.

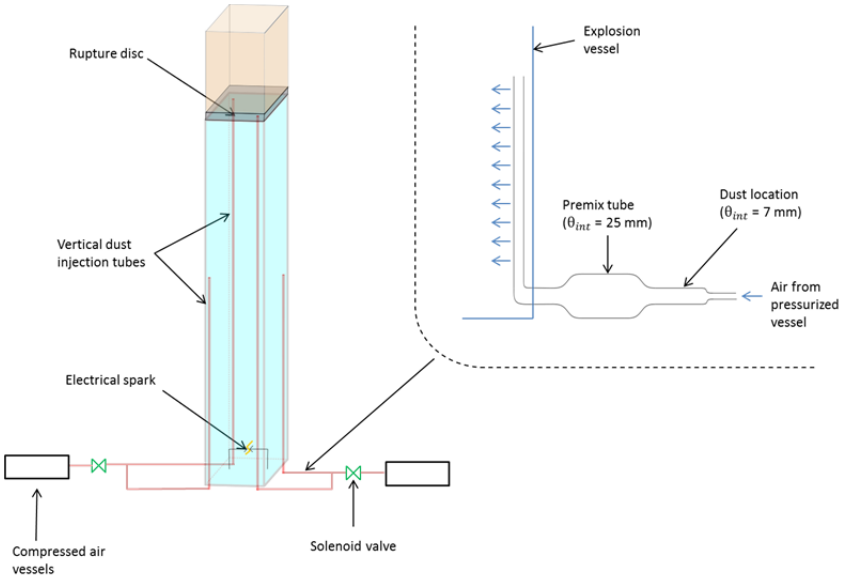

Figure 2: Schematic representation of the experimental apparatus elaborated for this study

The dust cloud is ignited by an electrical spark between two tungsten electrodes (diameter: 2.4 mm) located at the bottom of the tube. The distance between these electrodes is 4 mm. The spark is generated by a specific apparatus. First, this arc generator ionizes the air between the electrodes with a high-voltage transformer (20 kV), but this arc is not powerful enough (around 40 mJ: data from the constructor). Once the air is ionized, capacitors are discharged between the electrodes, leading to a powerful arc (several Joules). For the experiments presented in this paper, the intensity of the arc is 4 A and his duration is 99.9 ms. The measured energy is around 15 J.

A rupture disc is located at the top of the prototype, to limit the overpressure inside and to control the concentration. This latter is extensible. During the injection of the dust, the disc inflates to keep the atmospheric pressure inside the vessel at the moment of ignition. Besides, it has a weak rupture resistance to limit the overpressure. The flow is then conducted through an evacuation tube.

The experiments presented in this paper have been realized with the following protocol. First, dust is placed inside the injection tube (just after the solenoid valve), air vessels are pressurized up to 2.5 bar. The solenoid valves are then opened during 0.75 s. Then after another 0.75 s, the cloud is ignited by the electrical spark. The dust concentration is around 350 $g.m^{-3}$, calculated by measuring the amount of dust inside the tubes before and after each test.
To visualize the dust flame propagation by direct visualization, we used a Photron SA3, with a Nikkor 105 mm lens. The resolution is 1,024*512 pixels, 12bits dynamic with an acquisition frequency of 3800 fps and an exposure time of 2.5 µs. The region of interest is located from 30 to 60 cm from the bottom of the prototype.

3. Results

3.1 Images obtained

Images obtained during one test are presented on figure 3a. The flame is propagating from the bottom closed end to the upper open end. In this figure, the time between two images is 10 ms. These images are not saturated and permit to visualize the evolution of the flame front aspect over time. In figure 3b, the images obtained with a numerical saturation of the previous ones are presented. In this case, the flame propagation is also obtained but the details of the flame front are less visible: the flame front seems smoother.

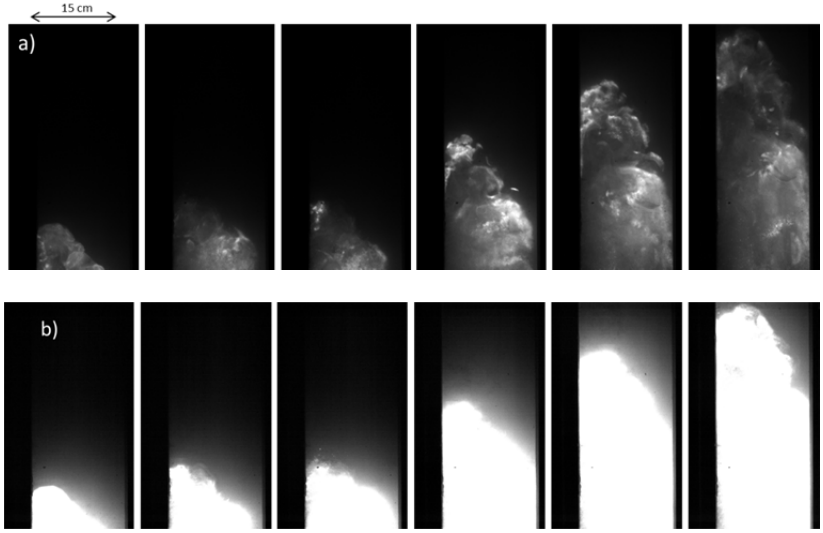

Figure 3: Images obtained of aluminum dust flame propagation (time between images: 10 ms), raw images (a) and numerically saturated images (b)

For the analysis of propagation and burning velocities, flame contour is estimated with an algorithm: based on Canny method for the non-saturated images and on thresholding for the saturated images (Canny, 1986). The determination of the flame contour is obviously somewhat arbitrary in both cases.

3.2 Propagation velocity

Figure 4 presents the evolution of the flame front position for each case, saturated and non-saturated images. The flame front position is defined as the vertical coordinate of the higher point of the estimated flame front contour. These two curves seem close, even if with saturated images the flame front position is slightly over-estimated at some times. This propagation can be separated in two stages. In the first, stage, the flame front propagates slowly and seems to stop propagating around 32 ms. Then the flame front starts to propagate faster, with a fairly constant velocity.
From these data of flame front position, the propagation velocity can be evaluated. Indeed, this velocity corresponds to the derivative of the position previously obtained. For the velocities evaluation, only the propagation after 32 ms is used. Figure 5 shows the propagation velocity for saturated and non-saturated images. For the case of saturated images, the propagation velocity seems to have more important fluctuations around the mean value. This is probably due to the fact that at some instants the flame front position seems to be over-estimated with these images. For non-saturated images, this propagation velocity varies from 3.9 to 5.7 m/s.

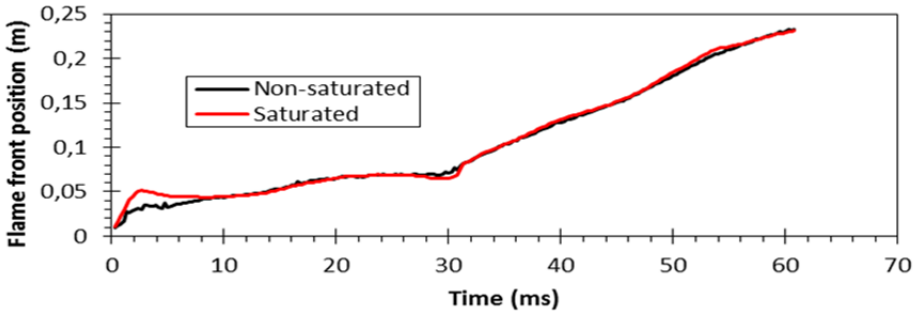

Figure 4: Evolution of the flame front position over time with saturated and non-saturated images

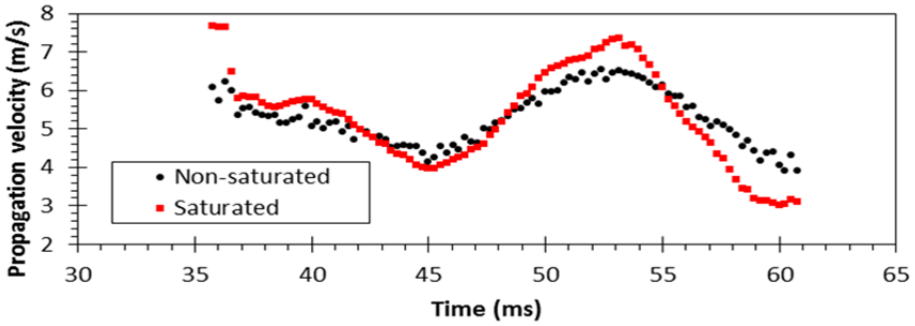

Figure 5: Evolution of the propagation velocity over time

3.3 Determination of burning velocity

The flame propagation velocity (V_p) corresponds to the flame speed in the laboratory referential. It is dependent on the geometry of the used apparatus. Another velocity is then derived from this previous one: the burning velocity, which corresponds to the consumption rate of the reactants by the flame front. The estimation of the burning velocity from the propagation velocity is achieved in two main steps.
First, as the flame propagates from the closed bottom end to the open top end of the prototype, propagation velocity is higher than burning velocity because of the thermal expansion of the burned gases. So, a first burning velocity S_u' can be defined from this correction:

$$Su' = \frac{V_p}{\chi} \quad (1)$$

Where χ is the thermal expansion coefficient, calculated as follow:

$$\chi = \frac{\rho_u}{\rho_b} \approx \frac{T_b}{Tu} \quad (2)$$

Where ρ_u and ρ_b are the densities of the unburned and burned gases respectively, T_u and T_b are respectively the temperature of the unburned gases (ambient temperature) and of the flame temperature (supposed adiabatic). The adiabatic flame temperature is obtained with the CEA (Chemical Equilibrium with Applications) Software (Gordon and McBride, 1994). In the conditions of the tests exposed in this article, this adiabatic flame temperature is 3,092 K leading to a thermal expansion coefficient of around 10.5.
Besides, burning velocity is defined as the propagation velocity of a planar flame. However, a planar flame is unstable. Therefore, another correction has to take into account the flame geometry (curvature effect). With this correction, the burning velocity S_u can be calculated from the previous velocity S_u' as follow:

$$Su = \frac{A'}{A_f}.Su' \quad (3)$$

Where A' is the projected flame area on a horizontal plane (corresponding to a virtual planar flame) and A_f is the flame surface. One major difficulty with this method consists on the determination of the 3D flame surface area from two-dimensional images of the flame. Here, the burning velocity is only determined in the phase of one-dimensional propagation (after the flame reaches the walls).

The method for the determination of the 3D flame surface from the recorded images is now presented in figure 6, extracted from Khalili (2012), considering that the flame profile is an ellipse on the plane perpendicular to the view plane. The procedure is as follow: first, the flame contour is estimated by image analysis (based on the Canny method or on thresholding). This contour is the red curve in the figure. Then, a circle (blue on the figure) is traced at the bottom of the flame profile. The unique ellipse (green on the figure) is then traced between each point of the flame front and this blue circle. From this 3D approximation of the flame front, the 3D flame surface area is then estimated.
With this methodology, the evolution of the flame surface area can be estimated from the images. For saturated images, the flame surface area is under-estimated of 10-20 %. It is consistent with the images shown in Figure 3. With saturated images, the flame front is smoother, so the flame surface area is less important.

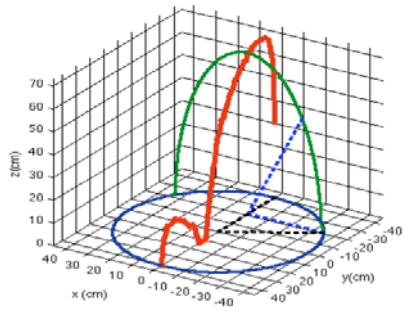

Figure 6: Methodology of flame surface area estimation, from Khalili (2012)

From the evolution of the flame front position and of the flame surface area, the burning velocity can be estimated, as shown by Figure 7. For saturated images, the value of the mean burning velocity is over-estimated: 24.5 cm/s for saturated images and 21.1 cm/s for non-saturated images. Besides, more important fluctuations, around this mean value, are observed for saturated images. Our results, especially with non-saturated images, are close to the data obtained by Goroshin et al. (1996b) with a bunsen burner, and by Julien et al. (2015) with unconfined propagation: see Table 1 (adapted of the analysis of Julien et al. (2017)). The difference with the data obtained by Goroshin et al. (1996a) also with the open tube method are possibly due to differences of initial turbulence level, not indicated in their work. In future work, the turbulence intensity will be evaluated and specified with each data of burning velocity, in order to compare to other studies.

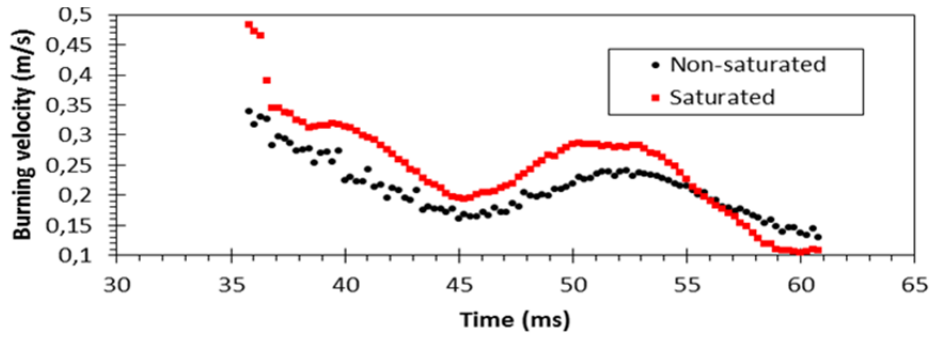

Figure 7: Evolution of the burning velocity over time

Table 1: Comparison of burning velocity data with the literature

Authors	Apparatus used	Burning velocity (cm/s)
(Goroshin et al., 1996b)	Bunsen burner	20
(Julien et al., 2017)	Conterflow burner	30-40
(Julien et al., 2015)	Unconfined propagation	20
(Goroshin et al., 1996a)	Open tube	30-40
Present study (Non-saturated)	Open tube	21
Present study (Saturated)	Open tube	25

4. Conclusions

This study focused on the visualization of aluminum dust flame propagation in a 15 L rectangular glass prototype. From images recorded in high speed, the burning velocity has been evaluated. The aim of the work was to compare the results obtained with non-saturated and with saturated images.

Saturated images yield to slightly over-estimated flame front position. The flame front surface area, also estimated with these images, was under-estimated compared to the surface area obtained with non-saturated. Indeed, with saturated images the flame front is smoother because less details of the flame front are detected. The resulting burning velocity is over-estimated with saturated images. So, saturated images should not be used for burning velocity determination, because of flame surface area under-estimation, especially in the case of turbulent flame propagation.

The complexity of the flame observed with the images obtained without saturation shows an eventual other limit of this technique. Depending, on the axe of visualization of the flame propagation, two different shapes of the flame contour can be obtained, and thus different determinations of the burning velocity. Tests are currently realized to visualize, for a same test, the propagation with another camera positioned at 90° from the first one. Then the results of burning velocity will be compared.

Even with non-saturated images, the evaluation of the flame contour, and so the flame surface area, is not easy, especially when the luminosity of the flame front changes with time. Thus, optical techniques such as schlieren or shadowgraph techniques should be preferred for flame surface evaluation. Moreover these two techniques are based on the visualization of refractive index variations, linked to temperature variations. Then a comparison of the direct visualization of the flame and the refractive index changes will be available while proceeding to common path recording in high speed of the dust explosion process.

Acknowledgments

The authors are grateful to IRSN (Institut de Radioprotection et Surete Nucleaire) for the scientific and financial support of this research project.

References

Canny, J., 1986, A computational approach to edge detection, IEEE Transactions on Pattern Analysis and Machine Intelligence, 8, 679-698.

Di Benedetto, A., Garcia-Agreda, A., Dufaud, O., Khalili, I., Sanchirico, R., Cuervo, N., Perrin, L., Russo, P., 2011, Flame propagation of dust and gas-air mixtures in a tube, Seventh Mediterranean Combustion Symposium.

Ding, Y., Sun, J., He, X., QuiHong, W., Yin, Y., Xu, Y., Chen, X., 2010, Flame propagation characteristics and flame structures of zirconium particle cloud in a small-scale chamber, Chinese Science Bulletin, 55, 3954-3959.

Dufaud, O., Khalili, I., Cuervo-Rodriguez, N., Olcese, R., Dufour, A., Perrin, L., Laurent, A., 2012, Highlighting the Importance of the Pyrolysis Step on Dusts Explosions, 26, 369–374, doi:10.3303/CET1226062

Gao, W., Mogi, T., Shen, X., Rong, J., Sun, J., Dobashi, R., 2014, Experimental study of flame propagating behaviors through titanium particle clouds, Science and Technology of Energetic Materials, 75, 14–20.

Gordon, S., McBride, B.J., 1994, Computer program for calculation of complex chemical equilibrium compositions and applications, NASA RP 1311.

Goroshin, S., Bidabadi, M., Lee, J.H.S., 1996a, Quenching distance of laminar flame in aluminum dust clouds, Combustion and Flame, 105, 147–160, doi:10.1016/0010-2180(95)00183-2

Goroshin, S., Fomenko, I., Lee, J.H.S, 1996b, Burning velocities in fuel-air rich aluminum dust clouds, Twenty-Sixth Symposium on Combustion, The Combustion Institue, 1961-1967.

Julien, P., Vickery, J., Goroshin, S., Frost, D.L., Bergthorson, J.M., 2015, Freely-propagating flames in aluminum dust clouds, Combustion and Flame, 162, 4241–4253, doi:10.1016/j.combustflame.2015.07.046

Julien, P., Whiteley, S., Soo, M., Goroshin, S., Frost, D.L., Bergthorson, J.M., 2017, Flame speed measurements in aluminum suspensions using a counterflow burner, Proceedings of the Combustion Institute, 36, 2291–2298, doi:10.1016/j.proci.2016.06.150

Khalili I., 2012, Sensibilité, sévérité et spécificités des explosions de mélanges hybrides gaz/vapeurs/poussières, PhD Thesis, Université de Lorraine, Nancy, France.

Proust, C., Veyssiere, B., 1988, Fundamental Properties of Flames Propagating in Starch Dust-Air Mixtures. Combustion Science and Technology, 62, 149–172, doi:10.1080/00102208808924007

Torrado, D., Cuervo, N., Pacault, S., Gaude, P.-A., Dufaud, O., 2017, Influence of carbon black nanoparticles on the front fl ame velocity of methane/air explosions, Journal of Loss Prevention in the Process Industries, 49, 919-928, doi:10.1016/j.jlp.2017.02.006